15

Rotor Fault Detection in Line-fed Induction Machines Using Complex Wavelet Analysis of Startup Transients

Fernando Briz, Michael W. Degner†, Pablo García,
David Díaz-Reigosa and Alberto Díez
University of Oviedo, †Ford Motor Company
Spain, †USA

1. Introduction

Three–phase inductions machines are the primary consumers of electric power in industrialized countries, they can typically consume between 40 to 50% of all the generated power (Thomsom et al., 2001). Diagnostic testing of induction machines is therefore of tremendous importance in many applications, and has been the focus of intense research for many years (Aller et al., 2002), (Antonino-Daviu et al., 2006), (Briz et al., 2008), (Benbouzid, 2000), (Douglas et al. 2003), (Douglas et al. 2004), (Douglas et al. 2005), (Douglas et al. 2005-b), (Faliang Niu & Jin Huang, 2005), (Nandi & Toliyat, 2005), (Thomson & Fenger, 2001), (Supangat et al., 2006).
Based on the results from failure surveys, the failure mechanism for induction machines can be divided into the following four general categories, with the percentage of total failure shown (Thomsom et al., 2001).

- Stator related: 40%
- Rotor related: 10%
- Bearing related: 40%
- Other: 10%

A number of methods have been developed for the purpose of detecting faults in induction machines, the ultimate goal being to prevent unexpected equipment downtime or severe equipment damage. Classification of the existing methods can be done according to several criteria, including:

- The type of fault that can be detected (stator, rotor, bearing, …).
- The physical quantities that are measured and further processed for the detection (phase currents, voltages, temperature, infrared, vibration, axial flux, acoustic noise, …).

This work was supported in part by the Research, Technological Development and Innovation Program of the Spanish Ministry of Science and Education-ERDF under grant MEC-ENE2007-67842-C03-01.

- If they work on-line or off-line. On-line methods do not stop the normal operation of the machine, while off-line methods require discontinuing the normal operation of the machine and often require moving it to a test rig.
- If they can work with constant and/or variable fundamental excitation, i.e., if they are valid for line-connected machines and/or inverter fed machines.

On-line methods are preferred in general for obvious reasons. Of special interest are methods that use terminal electrical quantities (currents/voltages), as they are easily measured. Methods of this type include negative sequence currents/impedances and motor current signature analysis (MCSA) (Kholer et al., 2002), (Lee et al., 2003), (Nandi & Toliyat, 2005), (Thomson & Fenger, 2001). These methods exploit the fact that an imbalanced machine, i.e., faulted, when fed with a balanced, three-phase voltage, produces specific components in the stator currents whose magnitudes and frequencies depend on the level of asymmetry and the cause of the fault condition.
Independent of their attractive properties, these methods have drawbacks that can limit their performance (Kholer et al., 2002), (Lee et al., 2003), (Nandi & Toliyat, 2005), (Thomson & Fenger, 2001). First, the line voltages feeding the machine often contain negative sequence components, which produce spurious current components caused not by imbalances in the machine but by the voltage feeding it. Although it is possible to measure the level of imbalance in the line voltages, it is not easy to accurately estimate their contribution to the overall current, since it depends on the machine's parameters and operating point. A second limitation of these techniques is the dependence of the fault related components on the operating point of the machine, and specifically, on the load level or slip. Several improvements have been proposed to mitigate these drawbacks (Lee et al., 2003), (Nandi & Toliyat, 2005).

1.1 Rotor fault detection

Rotor faults account for a relatively small portion (10%) of the overall failures occurring in induction machines. However, this portion is not uniform for all machines designs and applications. Broken rotor bars primarily occur in medium voltage motors with copper bar rotors. Direct line starting with heavy loads causes high thermal and mechanical stresses; pulsating mechanical loads such as reciprocating compressors or coal crushers (etc.) can subject the rotor cage to high mechanical stresses; an increased risk of rotor failure can exist in these cases (Loránd et al., 2004).
MCSA methods have successfully been applied to rotor fault detection. Damaged rotors produce spectral components in the stator current at frequencies that are function of the slip (and therefore of the rotor speed). The magnitude of these components is a function of the level of asymmetry of the rotor, from which the rotor condition can be evaluated. Regardless of its simple physical principles, use of MCSA for rotor fault detection presents limitations. When the machine operates with light load (small slips), the magnitude of the fault related components decrease, and their frequencies gets close to large fundamental excitation frequency related components, which result in them being difficult to separate. Also, oscillating loads or imbalances in coupled gears and/or mechanical transmissions can produce components in the currents at frequencies similar to those caused by faults, making them difficult to distinguish from a real fault.

The startup transient offers opportunities for performing rotor diagnostics of line-connected machines. When a machine is connected to the line, the startup transient is characterized by large stator (and rotor) currents, as well as by large slips (i.e., rotor speed significantly smaller than the excitation frequency). Damaged rotors create large rotor speed dependent components in the stator current during the startup transient. Analysis of the stator current of line-connected machines during startup provides, therefore, an excellent opportunity for performing rotor diagnostics.

Detection of damaged rotor bars using startup transients requires the use of methods capable of processing the transient signals. Wavelet functions are well suited for this purpose and wavelet based analysis has been proposed for machine diagnostics using startup transient currents (Aller et al., 2002), (Antonino-Daviu et al., 2006), (Briz et al., 2008), (Douglas et al. 2003), (Douglas et al. 2004), (Douglas et al. 2005), (Douglas et al. 2005-b), (Faliang Niu & Jin Huang, 2005), (Nandi & Toliyat, 2005), (Thomson & Fenger, 2001), (Supangat et al., 2006). In most of these works, *standard* wavelets transforms, i.e., wavelet families proven useful in other applications, are used. Discrete wavelet transform based filtering was used in (Aller et al., 2002), Daubechies-8 wavelet in (Douglas et al. 2003), (Douglas et al. 2004), (Douglas et al. 2005), (Douglas et al. 2005-b), (Supangat et al., 2006), Daubechies-40 wavelet in (Antonino-Daviu et al., 2006). In (Faliang Niu & Jin Huang, 2005), a continuous Morlet wavelet is proposed and the analysis was based on an estimate of the torque. This requires measurement of the stator voltage, as well as an estimate of the stator resistance, which significantly complicates the implementation of the method. A significant inconvenience of *standard* wavelets is that no clear criteria for selecting the wavelet function exist, with selection being made *ad hoc*. Also, although the wavelet based analysis can reveal differences between a healthy and a damaged machine, there is not a clear relationship between the physical characteristics of the signal and the results of wavelet based analysis.

Alternatively to the use of standard wavelets, it is possible to design wavelet transforms based on the physical properties exhibited by the currents when a damaged rotor exist (Briz et al., 2008). Since these wavelet respond to a known pattern, the design, as well as the selection of the parameters, are deterministic, with the interpretation of the results of the wavelet transform being straightforward.

A method for rotor fault detection using wavelet based analysis of the stator current complex vector during startup is presented in this work. The chapter is organized in 8 sections. Section 2 introduces the stator current complex vector of three-phase machines, with its nature during start-up transients for both healthy and faulty machines being discussed in section 3. Section 4 introduces complex vector wavelets designed to detect rotor fault related patterns of the stator current complex vector during the startup transient. Discussion on the design of the wavelet function, as well as experimental results demonstrating the viability and performance of the method are presented in Section 5. Section 6 analyses implementation aspects, the conclusions being presented in Section 7. Section 8 provides the reference list.

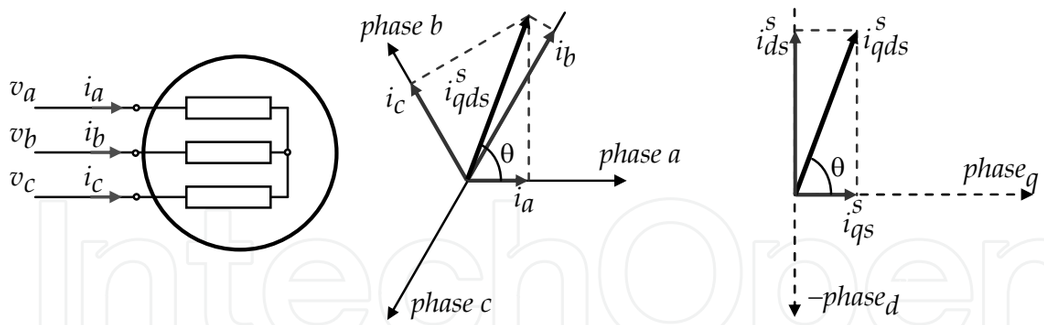

a) Three phase machine b) Three phase system c) Equivalent two-phase system

Fig. 1. Three phase machine and reference coordinates systems.

Table 1. Induction motor parameters (f_e = 50 Hz)

Power Rating	0.9 kW, 4 poles
V rated/ I rated (wye)	400 V / 2.3 A (rms)
Rated speed	1425 rpm
# Stator Slots / #Rotor Slots	24 / 30

2. The stator current complex vector

The stator current complex vector is the quantity measured and used in this work for detecting rotor faults in induction machines. This section provides a basic background on the definition and utilization of complex vector variables for the analysis of ac electric machines.

Complex vector quantities (or alternatively qd-axis models) are widely used for the analysis, design, control and diagnosis of three-phase, ac machines and three-phase power systems (Novotny & Lipo, 1996). Given a set of three-phase currents i_a, i_b and i_c (Fig. 1a), the stator current complex vector is defined as:

$$i^s_{qds} = i^s_{qs} - \mathrm{j}\, i^s_{qd} = \frac{2}{3}\left(i_a + i_b\, \mathrm{e}^{\mathrm{j}2\pi/3} + i_c\, \mathrm{e}^{\mathrm{j}4\pi/3} \right) \quad (1)$$

The transformation in (1) can be visualized as the currents i_a, i_b and i_c aligned with three non-orthogonal axes with a phase shift of 120º from each other (Fig. 1b), being transformed to an orthogonal *q-d* reference frame (Fig. 1c). The stator current complex vector (1) can be represented as a complex quantity or in cartesian form by using its real and imaginary components, i^s_{qs} and i^s_{ds} respectively.

Fig. 2a shows the three phase stator currents of the test machine operating in the steady-state. The parameters of the machine are shown in Table I. Fig. 2b shows the resulting q- and d-axis components obtained using the transformation defined by (1), while Fig. 2c

shows the trajectory of the resulting complex vector. For the case of balanced, sinusoidal three-phase currents, the stator current complex vector consists of a *single rotating component*, with its magnitude being equal to the peak value of the phase currents, its frequency of rotation coinciding with the frequency of the phase currents.

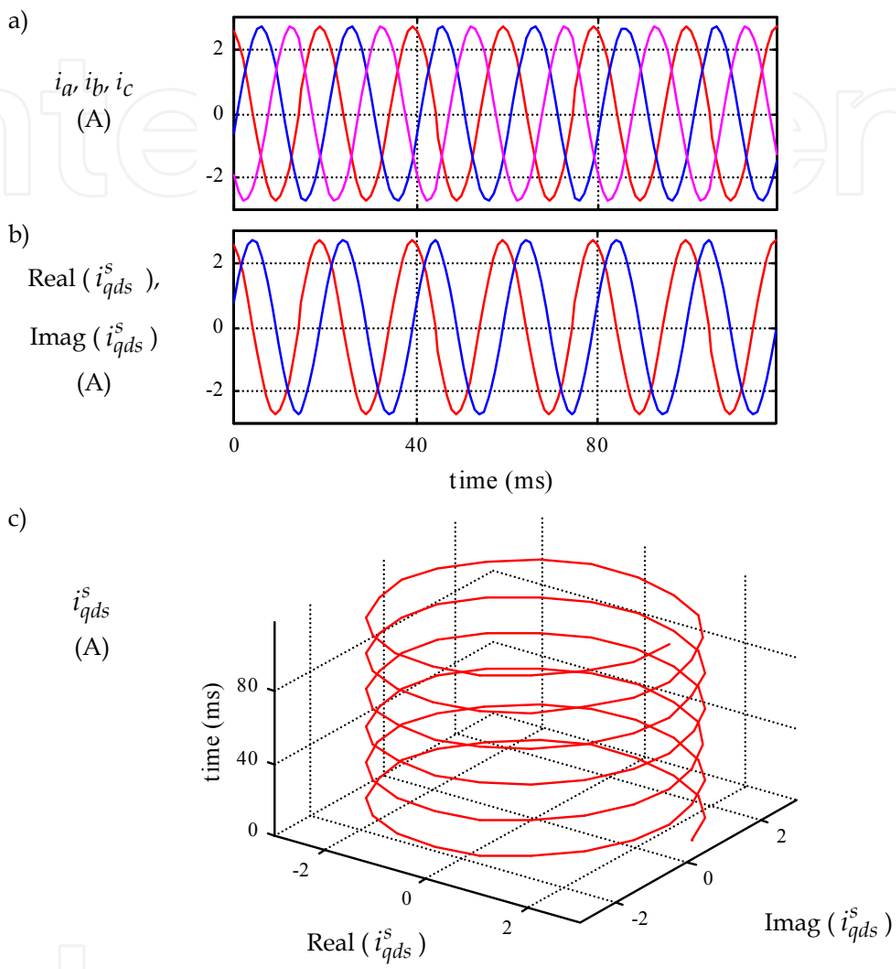

Fig. 2. a) phase current i_u, i_v, i_w, b) q and d-axis components of the stator current complex vector, and c) trajectory of the stator current complex vector with the machine operated in steady-state.

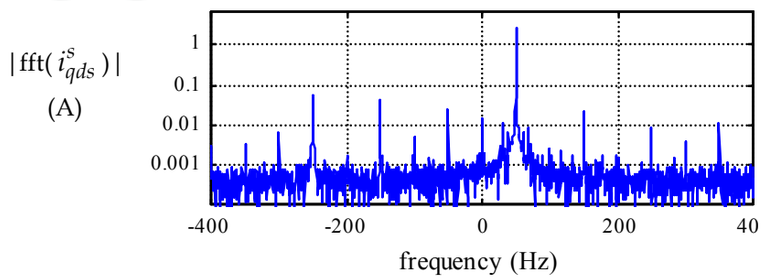

Fig. 3. Frequency spectrum (only magnitude) of the stator current complex vector.

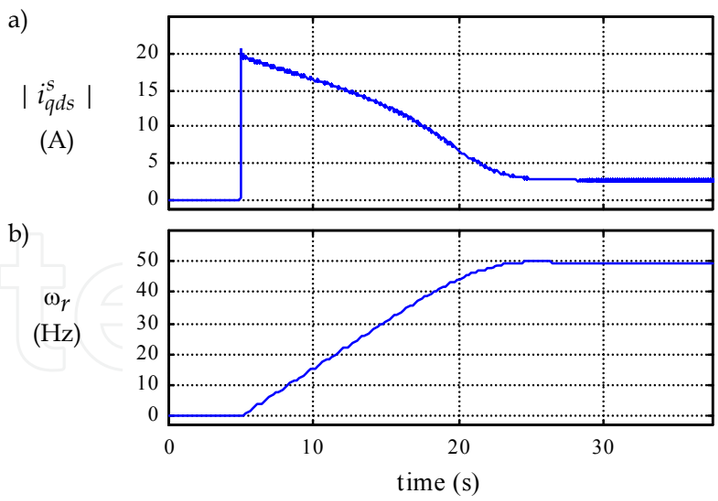

Fig. 4. a) Magnitude of the stator current complex vector and b) rotor speed during startup (400 V rms, 50 Hz), with the motor driving a large inertia load.

Fig. 3 shows the frequency spectrum of the stator current complex vector. Since it is a complex vector quantity, its frequency spectrum contains both positive (forward rotating) and negative (backward rotating) frequency components. It can be observed from the figure that the largest component is at a frequency of ω_e=50 Hz, which corresponds to the fundamental (line) frequency, with a number of additional harmonics of relatively small magnitude being also observable both at positive and negative frequencies.

3. Analysis of the stator current complex vector during startup

Fig. 4 shows the stator current complex vector magnitude and the rotor speed of the test machine after it was connected to the line. Since the transient stator current complex vector after connection is a non-stationary signal, conventional FFT based analysis of the type shown in Fig. 3 is not adequate. Instead, the Short Time Fourier Transform (STFT) can be used for these purposes (Benbouzid, 2000), (Briz et al., 2008). Fig. 5a shows the spectrogram of the stator current complex vector (1), obtained using the STFT, during the transient shown in Fig. 4, for the case of a healthy machine. A sampling frequency of 5 kHz, with a window width of 2048 samples was used.

The most significant component in the spectrogram is at the line frequency, ω_e=50 Hz, and corresponds to the fundamental current. Additional components of reduced magnitude (note the logarithmic scale of the color bar) can also be observed. Horizontal lines correspond to components that do not vary with the rotor speed and have several physical origins, e.g., saturation; additional components in the line voltages; interactions between the fundamental excitation and asymmetries intrinsic to the design of the machine; imbalances in the measurement circuits (current sensors and further electronics), etc. All of these components generally have a small magnitude compared to the signals of interest but they are still visible when a logarithmic scale is used (Briz et al., 2008).

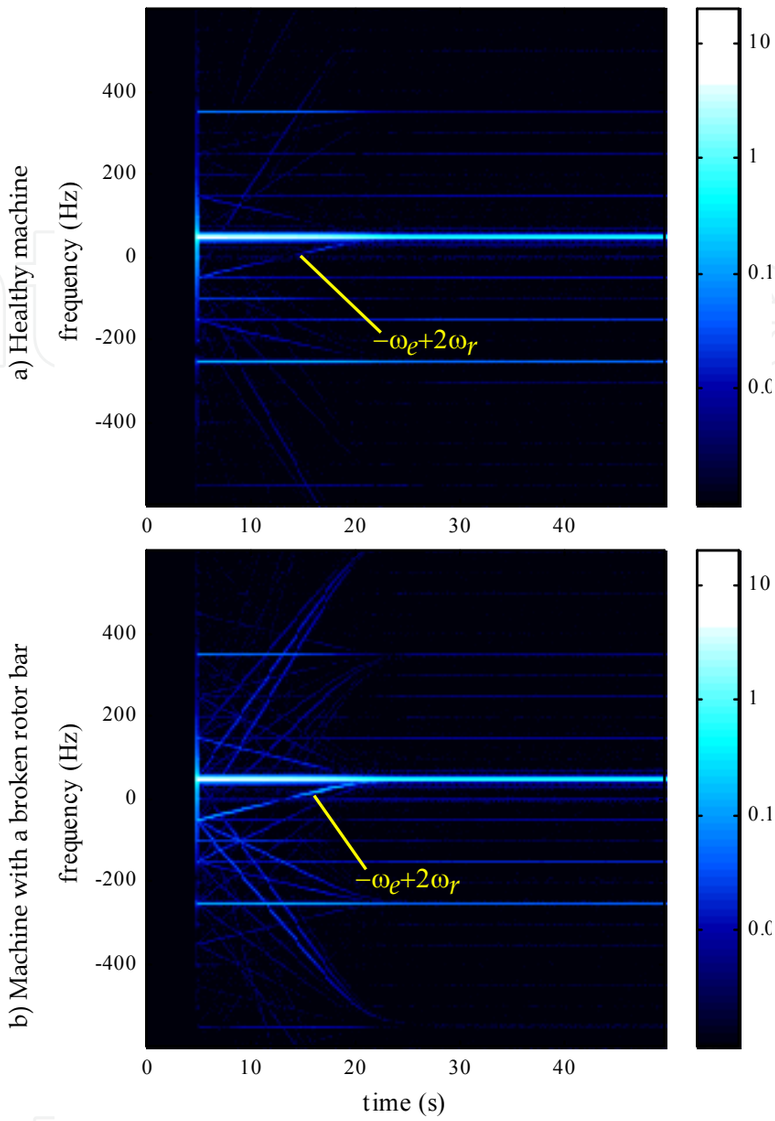

Fig. 5. Spectrogram of the stator current complex vector during startup with the motor driving a large inertia load, for the case of a) a healthy machine and b) machine with a broken rotor bar. Color bar units: Amps.

Rotor speed dependent components can also be observed in the spectrogram. Such components have previously been reported even for the case of healthy machines due to design and construction asymmetries (Benbouzid, 2000).

Fig. 5b shows the spectrogram of the stator current complex vector during a startup transient for the case of a machine with a broken rotor bar. The bar was *disconnected* by drilling the end ring, as shown in Fig. 6. The rotor was modified so that the continuity of the end-ring was maintained and the rotor laminations were not affected. Components of the stator current complex vector caused by a damaged rotor bar are given by (2) (Benbouzid, 2000), where ω_e is the electrical frequency, s is the slip, p the number of pole pairs,

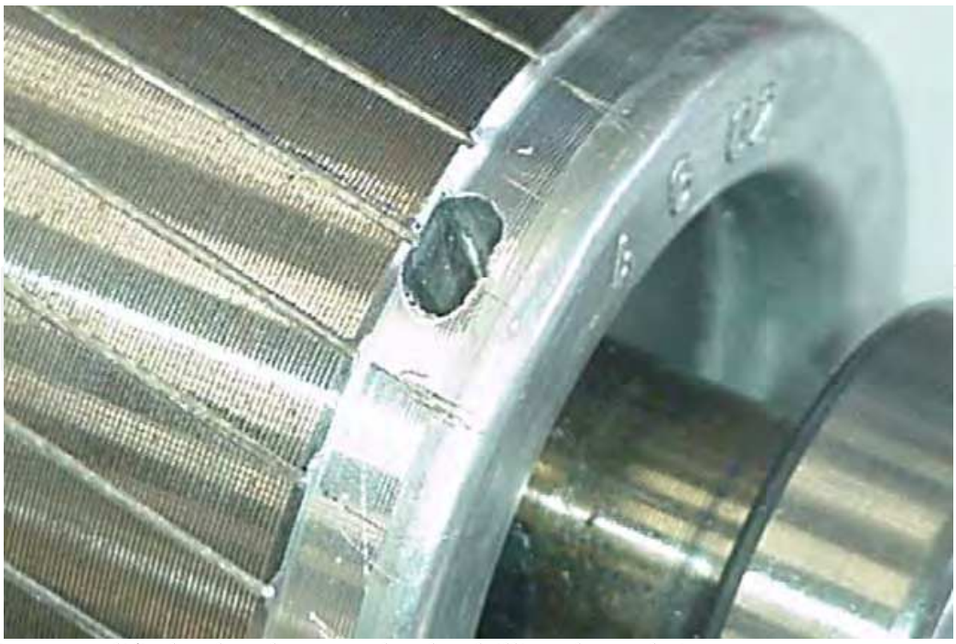

Fig. 6. Rotor modified to break a rotor bar by drilling the end-ring.

and with k/p = 1, –5, 7, –11, 13, … . The most important component, (3), denoted as ω_{brb-2}, is obtained from (2) with k/p = 1.

$$\omega_{brb} = \omega_e \left(k \frac{(1-s)}{p} \pm s \right) \tag{2}$$

$$\omega_{brb-2} = \omega_e (1-2s) = -\omega_e + 2\,\omega_r \tag{3}$$

Using (2) and (3), the stator current complex vector can be modeled as (4), where the first term on the right hand side represents the current of a healthy machine, while the rest of the terms represent the rotor fault-induced components.

$$i^s_{qds} = i^s_{qds\ healthy} + I_{brb-2}\, e^{j(-\theta_e + 2\theta_r)} + \Sigma I_{brb-k}\, e^{j((-\theta_e + 2\theta_r)k/p)} \tag{4}$$

It can be seen from Fig. 5b that rotor speed dependent components that are readily observable during the startup transient have a significantly reduced magnitude in the steady-state. In addition, all of the rotor speed dependent components converge to frequencies in the steady-state that are spectrally close to the fundamental excitation frequency or its harmonics. This makes their separation in the steady-state difficult, especially if the machine is not heavily loaded. It can be concluded then that significantly richer information for revealing a damaged rotor exists in the current vector during startup than exists during steady-state operation.

4. Detection of damaged rotor bards using complex vector wavelets

The separation of the information revealing a damaged rotor from the overall stator current requires adequate signal processing. The STFT, combined with a spectrogram representation of Fig. 5 is one option. However, while visually insightful, it is not easy to establish a metric that indicates the rotor condition. Wavelets are an efficient tool for pattern detection in transient signals. This can be accomplished by designing the wavelet to resemble the attributes of the signal to be detected.

4.1 Wavelet design

It has been shown that a damaged rotor induces, among others, a component, I_{brb-2} (4), in the stator current complex vector. This component is resembled during a startup transient by a wavelet function ψ, (5), consisting of a complex exponent multiplied by a windowing function, *h*.

$$\psi(t) = h(t)\, e^{\,j((tq_e(t)+2q_r(t))} \tag{5}$$

The complex exponent is a function of the electrical angle, θ_e and the rotor angle, θ_r. These angles can be obtained by integration of the fundamental excitation frequency, ω_e, and the rotor speed, ω_r, respectively, (6). However, while ω_e is known in advance and constant, ω_r is practically never measured in line-connected machines. Because of this, an estimate of the rotor speed during the startup transient ω_{rw} needs to be used. For this work, the estimate $\omega_{rw}(t)$ was obtained using a simple polynomial curve fit method from the $-\omega_e+2\omega_r$ component in the spectrogram shown in Fig. 5a during a commissioning stage, the estimated rotor speed being shown in Fig. 4b. The angle θ_{rw} was then obtained by integrating $\omega_{rw}(t)$ (6).

$$\theta_e(t) = \int \omega_e \, dt \,, \;\; \theta_{rw}(t) = \int \omega_{rw}(t) \, dt \tag{6}$$

It is noted that the determination of the exact value of $\omega_{rw}(t)$ is not critical, as the wavelet (5) will later be scaled (i.e., stretched or shrunk) to effectively sweep the expected range of startup transient time lengths and shifted to find the exact time in which the startup transient occurred. This is done by defining θ_{rw} (7) and *h* as a function of *scale* (denoted as *a*) and *time translation* (denoted as *b*) (discussion about the design of *h* is presented in sub-section 4.3). The resulting wavelet function is given by (8).

$$\theta_{rw}(a,b) = \int \omega_{rw}((t-b)/a) \, dt \tag{7}$$

$$\psi(a,b) = h(a,b)\, e^{\,j\,(tq_e+2q\theta_{rw}(a,b))} \tag{8}$$

Since the wavelet definition (8) relies on an estimation of the *rotor speed shape*, the reliability of the method can be reduced if significant variations in the *rotor speed shape*, due to variations

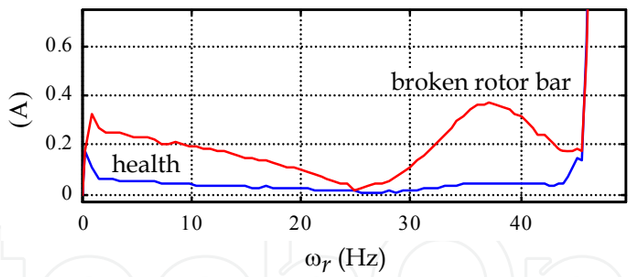

Fig. 7. Magnitude of the stator current complex vector component at $-\omega_e+2\omega_r$ (I_{brb-2} in (4)) vs. ω_r for the case of a healthy machine and a machine with a broken rotor bar, during the startup transients of Fig. 5.

in the load characteristics, occur. It is emphasized however that variations of the transient length do not prevent the method from providing reliable fault detection, as will be demonstrated in section 5.

4.2 Wavelet transform

Once ψ is defined, (8), the coefficient of the wavelet transform C is obtained using (9) (MathWorks Inc., 2007), with '*' standing for the complex conjugate. It is noted that, although the integral symbol is used in (9), it actually operates with sampled signals, with the integration being transformed into a summation in the practical implementation.

$$C(a,b) = \frac{1}{\sqrt{a}} \int \psi^*(a,b)\, i^s_{qds}\, dt \tag{9}$$

This coefficient is a function of a, i.e., how much the base wavelet is stretched or shrunk, and b, i.e., how much the wavelet is shifted in time with respect to the signal being analyzed. Evaluation of (9) is made by changing a and b at short, regular steps, resulting therefore in a *continuous wavelet transform* (MathWorks Inc., 2007).

Selecting a and b in (9) is straightforward since they are directly related to characteristics of the signal being analyzed. The limits for a are related to the minimum and maximum startup transient time lengths, while the limits for b are related to how accurately the startup transient can be detected.

4.3 Selection of the windowing function

The windowing function h in (5) is required so that the wavelet, ψ, has a finite length and a smooth transition, since the complex exponential term in (5) has a constant magnitude equal to one. Fig. 7 shows the magnitude of the stator current complex vector $-\omega_e+2\omega_r$ component vs. ω_r for the case of a healthy machine and for the case of a machine with a broken rotor bar. They were obtained from signal processing of the spectrograms in Fig. 5a and 5b, respectively. It is interesting to notice that while the differences between the two signals are noticeable during the startup transient, both signals increase significantly and coincide for values of ω_r near ω_e (50 Hz). This is due to the fact that the frequency being tracked (3)

approaches the fundamental frequency of the current, which has a much larger magnitude

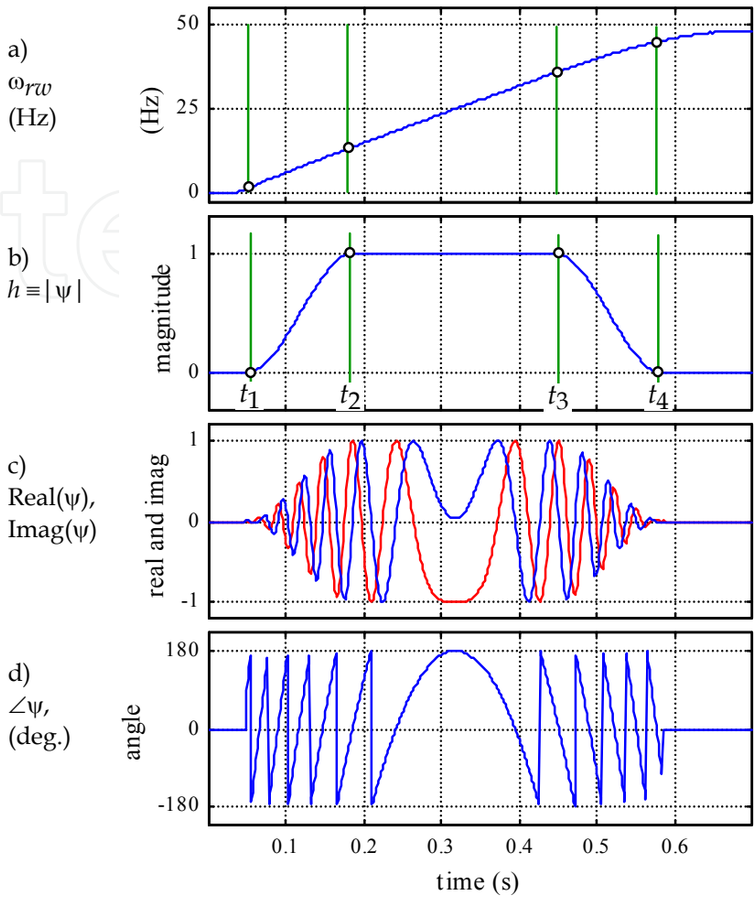

Fig. 8. Construction of the complex vector wavelet, ψ. a) estimated rotor speed, b) windowing function, *h*, c) real and imaginary components of ψ, and d) phase angle of ψ.

and is difficult to separate from the desired signal. A similar effect is also observed for values of ω_r near 0, caused by the spectral closeness of the $-\omega_e$ component.

To avoid *border effects*, *h* is chosen to be equal to zero for values of ω_{rw} near 0 and ω_e. This is schematically shown in Fig. 8. The window has two transition regions (t_1–t_2 and t_3–t_4) of variable magnitude and a mid-region (t2–t3) of constant magnitude. The transition regions are defined by (10)-(11), being similar to a *hanning* window. The real and imaginary components of the resulting wavelet function, (5), are shown in Fig. 8c, with its magnitude and phase in Fig. 8b and 8d, respectively.

$$h_{12} = \frac{1 - cos(\alpha_{12})}{2}, \text{ with } \alpha_{12} = \frac{(t - t_1)\pi}{(t_2 - t_1)} \text{ and } t_1 < t < t_2 \tag{10}$$

$$h_{34} = \frac{1 + cos(\alpha_{34})}{2}, \text{ with } \alpha_{34} = \frac{(t - t_3)\pi}{(t_4 - t_3)} \text{ and } t_3 < t < t_4 \quad (11)$$

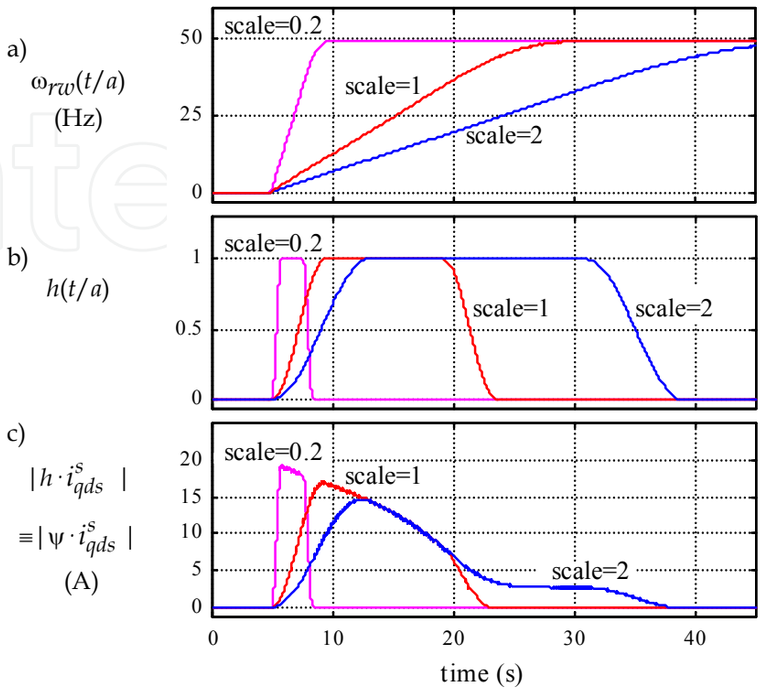

Fig. 9. a) Estimated rotor speed, b) windowing function and c) magnitude of windowed stator current complex vector resulting from applying the windowing functions to the stator current complex vector magnitude of Fig. 1. In all cases b=0.

Although this window will be used for all of the experimental results presented in this work, a variety of windowing functions can be used, each providing similar results (Briz et al., 2008).

5. Experimental verification of the method

The proposed method was tested using the machine in Table I. Fig. 9a and 9b shows the estimated rotor speed ω_{rw} and the windowing function, h, defined by (10)-(11), for different scales of a, with 0.2 and 2 representing the limits over which the wavelet transform (9) was evaluated, and 1 being a nominal case. Fig. 9c shows the magnitude of the windowed stator current complex vector for these values of a.

Fig. 10a and 10b show the magnitude of the C coefficient resulting from the wavelet transform for the case of a healthy machine and a machine with a broken rotor bar respectively. The estimated start of the transient was assigned a time t=0, the b (*time translation*) parameter of the wavelet transform, ψ, being evaluated in a range of –0.2 to 0.3 s around this value. The a parameter was varied within a range of 0.2 to 2 times the base function. The region of Fig. 10b that shows the most significant differences with respect to Fig. 10a is zoomed. Comparing Fig. 10a and 10b it can be observed that the coefficient of the

wavelet transform for the case of a healthy machine (Fig. 10a) has a rather constant value (uniform color), independent of the values for *a* and *b*. This means that the wavelet transform

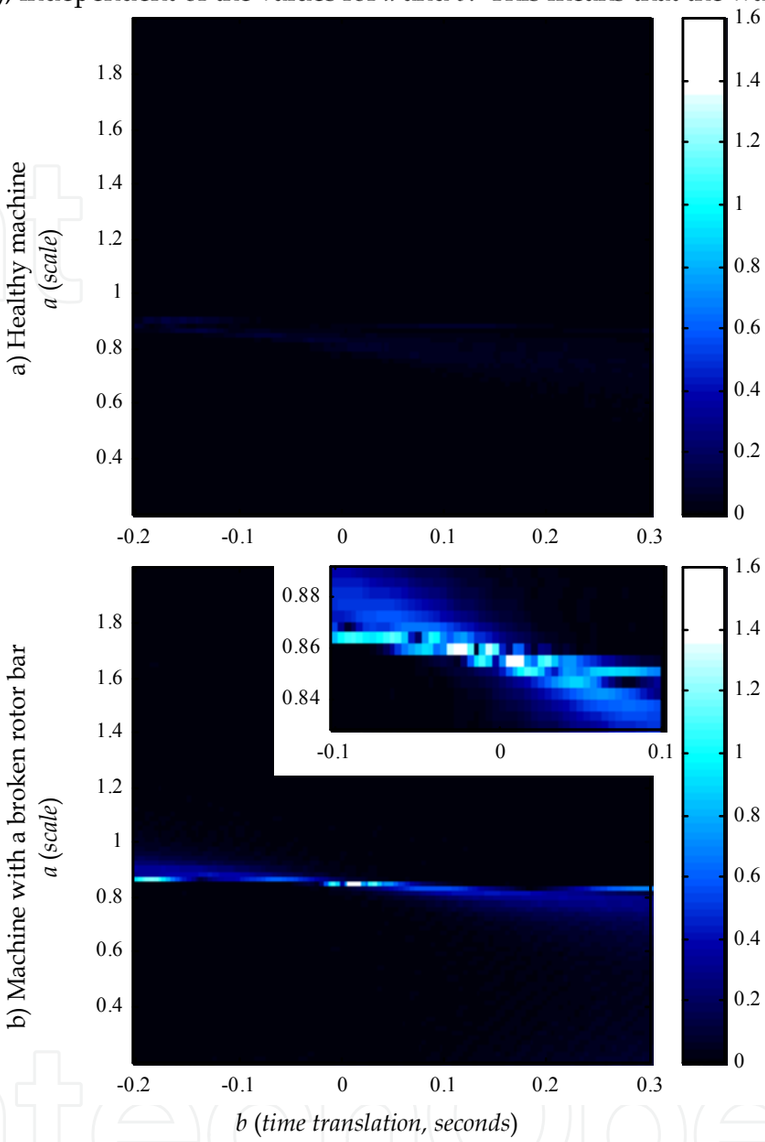

Fig. 10. Magnitude of the wavelet transform coefficient $|C|$ during the startup transient shown in Fig. 9, as a function of *a* and *b* (relative to the estimated start of the transient).

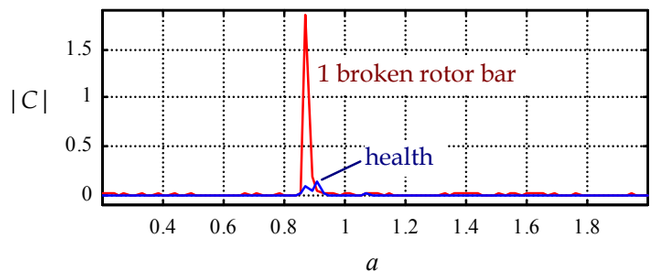

Fig. 11. Magnitude of the wavelet transform coefficient $|C|$ during a startup transient, as a

function of *a* (*scale*), (*b*=–0.04 s), for the case of a healthy machine and a machine with a broken rotor bar.

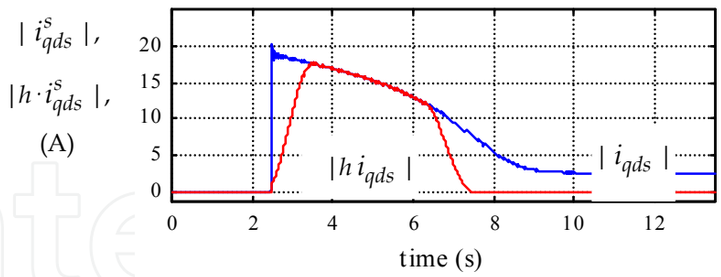

Fig. 12. Magnitude of the stator current complex vector and of the windowed stator current complex vector during startup transient.

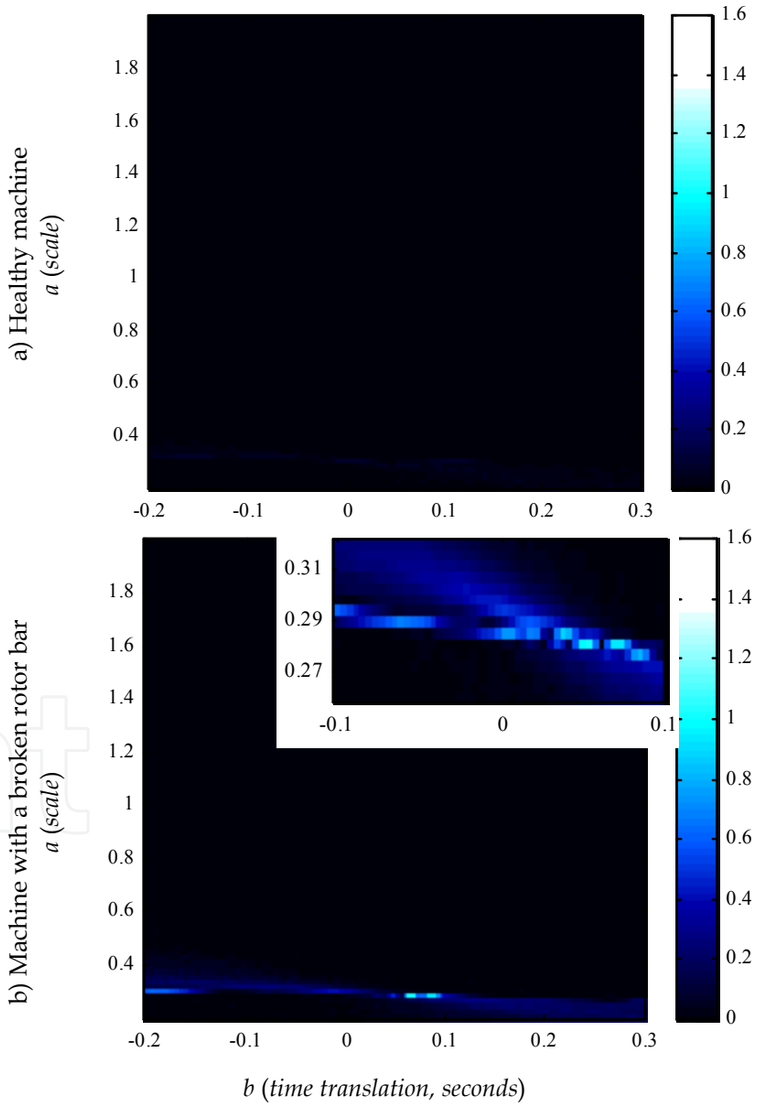

Fig. 13. Magnitude of the wavelet transform coefficient $|C|$ during the startup transient shown in Fig. 12, as a function of *a* and *b* (relative to the estimated start of the transient).

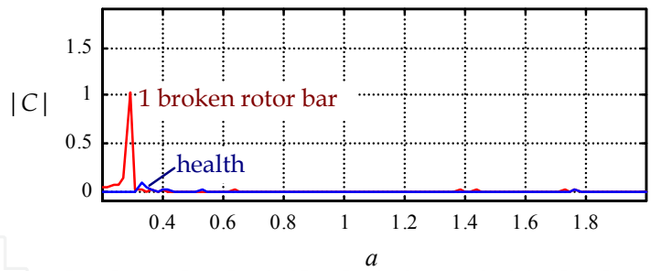

Fig. 14. Magnitude of the wavelet transform coefficient $|C|$ during a startup transient, as a function of a (*scale*), (b=–0.04 s), for the case of a healthy machine and a machine with a broken rotor bar.

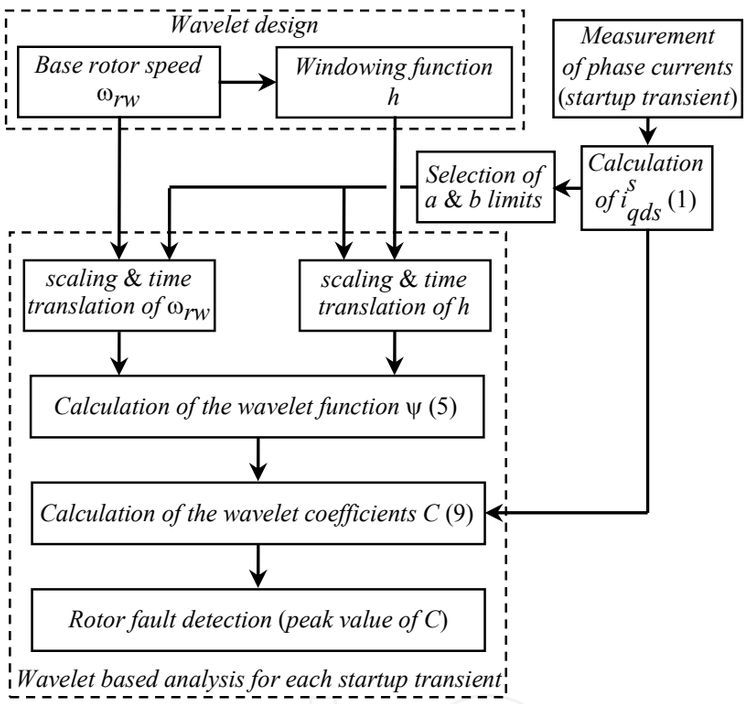

Fig. 15. Flowchart showing the implementation of the method.

effectively *eliminates* components of the stator current complex vector different from the one modeled by the wavelet function ψ. On the other hand, the coefficient C resulting from the wavelet transform for the case of a machine with a broken rotor bar has large values for well defined values of a and b, which reflects that good correlation exists between the wavelet, ψ, and the signal for these values of a and b.

Fig. 11 shows the value of C, as a function of a, from Fig. 10 for b=–0.04 s, for the cases of a healthy machine and a machine with a broken rotor bar. It can be observed that the maximum value of C is obtained for a=0.86, i.e., the startup transient was shorter than the wavelet base function.

It is concluded from these results that the proposed wavelet transform is highly sensitive to the properties exhibited by the current of a motor with a damaged rotor during startup. A metric as simple as the peak value of $|C|$ can be used to effectively indicate the condition of the machine.

5.1 Influence of the start up transient length

To assess the robustness of the method against variations in the startup transient characteristics, the analysis was repeated with the machine driving a significantly smaller inertia. Fig. 12 shows the magnitude of the stator current complex vector during the startup, as well as the windowed current. Fig. 13a and 13b shows the magnitude of the coefficient, C, for the case of a healthy machine and of a machine with a broken rotor bar, respectively. Regardless of the significant change in the startup transient's length, the wavelet transform in Fig. 13b clearly displays the presence of a fault. Fig. 14 shows the values of C, as a function of a, for b= 0.06 s, both for the healthy machine and for the machine with a broken rotor bar.

6. Implementation of the method

The proposed method requires the measurement of three current sensors for the implementation described in Section 3 (see Fig. 1a). The use of two current sensors is adequate for these purposes, however, and is a common practice, provided that no zero sequence current exists. It is equally valid for both delta- and wye-connected machines, and for machines with open as well as closed rotor slots. For the experiments presented in this work, conventional Hall effects current sensors and 12 bits A/D converters were used.

Fig. 15 shows the flowchart of the method. For the wavelet design, the rotor speed, ω_{rw}, during a startup transient is estimated and stored. The windowing function, h, is then designed as discussed in Section 5 and stored for later use. The stored ω_{rw} and h are then used for the wavelet based analysis each time that a startup occurs.

The peak value of $|C|$, is used to indicate the condition of the machine. This implies the establishment of a threshold that differentiates a healthy from a faulty machine. This cannot be easily done when no previous data from the machine of interest exists. It is recommended that C_{peak} be measured when a machine is first installed, or is known to be healthy, after that, increments or changes in the value of C_{peak} would indicate a deterioration of the rotor. Tracking the changes in C_{peak} could also be used for diagnostics in machines already installed and for which the condition of the rotor is unknown (with the assumption that the rotor starts out relatively healthy and any increase in C indicates a deterioration in the rotor bar health).

The experimental results shown in Fig. 10 and 13 used a wide range of values for a and b to better show the results of the method. However, to reduce the computational and time requirements of the method, the range of evaluation for a and b parameters can be significantly reduced by simple analysis of the startup transient current vector magnitude (Fig. 4 and 12). The start of the transient can typically be accurately established, which suggests that b could be restricted to a single value. However, it is convenient in practice to allow a narrow range of evaluation for b. This allows for compensation of effects like those

caused by the non-ideal (non-repetitive) behavior of the breakers, the variation of the instant in time relative to the period of the phase voltages in which the breakers were ordered to close, as well as for inaccuracies in the rotor speed ω_{rw}. For the experiments presented in this paper, the time translation parameter b was changed in steps of 5 ms, with a range of variation in the order of ±0.1 s relative to the theoretical start of the transient.
As for the selection of the range of a, line-connected machines often show repetitive startup transients, allowing for narrow bounds to a, which would be specific for each application. For the case of machines showing significant variations in the startup transient length, simple threshold based analysis of the startup current can be used to dynamically adapt the limits for a for each startup transient. For the experiments presented in this paper, a was changed in steps of 0.02. The calculation of the C coefficient for each value of a and b, including scaling of h and ω_{rw}, took ≈0.06 s in a standard computer.
In the top-right corner of Fig. 10b and 13b the wavelet transform coefficient is shown with a and b restricted to a reduced range of values, which were automatically obtained by the analysis of startup transient current described above.

7. Conclusion

Broken rotor bar detection in a line-connected induction machine using complex wavelets to analyze the stator currents during startup transients was presented in this work. These wavelets allow for the accurate detection of fault related components in the stator current complex vector indicative of damaged rotors. In comparison with standard wavelet based methods, the wavelet design is made following a well defined procedure. Because of this, limits for the *scale* and *time translation* parameters of the transform are easily established, reducing the computational requirements of the transformation. In addition, interpretation of the results of the wavelet transform is physically insightful. Experimental results confirm the effectiveness of the method in detecting damaged rotor bars.

8. References

Aller, J. M., Habetler, T. G. , Harley, R. G. , Tallam, R. M. , and Lee, S. B. ,"Sensorless Speed Measurement of AC Machines using Analytic Wavelet Transform," *IEEE Transactions on Industry Applications*, vol. 38, pp. 1344–1350, Sept./Oct. 2002.

Antonino-Daviu, J.A., Riera-Guasp, M., Folch, J.R.; Palomares, M.P.M., "Validation of a new method for the diagnosis of rotor bar failures via wavelet transform in industrial induction machines", *IEEE Transactions on Industry Applications*, vol. 42, no. 4, pp:990–996, July-Aug. 2006.

Benbouzid, M.E.H., "A review of induction motors signature analysis as a medium for faults detection", *IEEE Transactions on Industrial Electronics.*, vol. 47, no 5, Oct. 2000, pp 984-993.

Briz, F., Degner, M. W. , García, P., Bragado, D., "Broken Rotor Bar Detection in Line-fed Induction Machines Using Complex Wavelet Analysis of Startup Transients", *IEEE Transactions on Industry Applications*, vol.: 44, nº 3, pp. 760-768, May. 2008.

Douglas, H.; Pillay, P.; Ziarani, A., "Detection of broken rotor bars in induction motors using wavelet analysis"; *IEEE International Electric Machines and Drives Conference IEMDC'03*, Vol. 2, pp: 923–928, June 2003.

Douglas, H.; Pillay, P.; Ziarani, A.K., "A new algorithm for transient motor current signature analysis using wavelets", *IEEE Transactions on Industry Applications*, vol 40, no. 5, Sept. 2004, pp 1361-1368.

Douglas, H.; Pillay, P., "The Impact of Wavelet Selection on Transient Motor Current Signature Analysis", *IEEE-International Conference on Electric Machines and Drives IEMDC*, 2005 pp 80-85.

Douglas, H., Pillay, P. and Ziarani, A. K. , "Broken Rotor Bar Detection in Induction Machines with Transient Operating Speeds," *IEEE Transactions on Energy Conversion*, vol. 20, no. 1, pp. 135-141, March 2005.

Faliang Niu; Jin Huang, "Rotor broken bars fault diagnosis for induction machines based on the wavelet ridge energy spectrum", *Proceedings of the Eighth International Conference on Electrical Machines and Systems ICEMS 2005*, Vol. 3, pp:2274 – 2277, Sept. 2005.

Kohler, J.L., Sottile, J., Trutt, F.C., "Condition Monitoring of Stator Windings in Induction Motors: Part I-Experimental Investigation of the Effective Negative-Sequence Impedance Detector", *IEEE Trans. on Ind. Appl.*, vol. 38, no. 5, pp 1447 – 1453, Sept. 2002.

Lee, S.B., Tallman, R.M., Habetler, T.G.,"A Robust, On-Line Turn-Fault Detection Technique for Induction Machines Based on Monitoring the Sequence Component Impedance Matrix", *IEEE Trans. on Power Electron*, vol. 18, nº 3, pp. 865-872, May 2003.

Loránd, S., Dobai, J.B., Biró, K.A., "Rotor faults detection in squirrel-cage induction motores by current signature analysis", *IEEE-TTTC-International Conference on Automation, Quality and Testing, Robotics*, May 13–15, 2004, Cluj-Napoca, Romania.

MathWorks Inc., *Wavelet Toolbox User's Guide*, Natick, MA, 2007.

Nandi, S.; Toliyat, H.A., "Condition monitoring and fault diagnosis of electrical machines-a review", *IEEE Trans. on Energy Conversion*, vol. 20, no 4, Dic. 2005, pp 719-729.

Novotny, D.W., Lipo, T.A., *Vector Control and Dynamics of AC Drives*, Oxford University Press, New York, 1996.

Supangat R., Ertugrul N., Soong W.L., Gray D.A., Hansen C. and Grieger J., "Detection of Broken Rotor Bars in Induction Motor using Starting-Current Analysis and Effects of Loading," *IEE Proceedings - Electric Power Appications*, Vol. 153, No. 6, November 2006.

Thomson, W.T., Fenger, M., "Current Signature Analysis to Detect Induction Motor Faults", *IEEE Industry Applications Magazine*, May/June 2001, pp. 26-34.

Fault Detection

Edited by Wei Zhang

ISBN 978-953-307-037-7
Hard cover, 504 pages
Publisher InTech
Published online 01, March, 2010
Published in print edition March, 2010

In this book, a number of innovative fault diagnosis algorithms in recently years are introduced. These methods can detect failures of various types of system effectively, and with a relatively high significance.

InTech Europe
University Campus STeP Ri
Slavka Krautzeka 83/A
51000 Rijeka, Croatia
Phone: +385 (51) 770 447
Fax: +385 (51) 686 166
www.intechopen.com

InTech China
Unit 405, Office Block, Hotel Equatorial Shanghai
No.65, Yan An Road (West), Shanghai, 200040, China
中国上海市延安西路65号上海国际贵都大饭店办公楼405单元
Phone: +86-21-62489820
Fax: +86-21-62489821

IntechOpen